Journal of Catalysis **190,** 284–295 (2000)
doi:10.1006/jcat.1999.2745, available online at http://www.idealibrary.com on IDEAL®

Molecular and Temperature Aspects in Catalytic Partial Oxidation of Methane

Luca Basini,[1] Alessandra Guarinoni, and Aldo Aragno

Snamprogetti S.p.A. Research Laboratories, Via Maritano 26, 20097 San Donato Milanese (Milan), Italy

Received July 13, 1999; revised October 29, 1999; accepted October 29, 1999

Heterogeneous stoichiometric oxidation and catalytic partial oxidation (CPO) of methane are studied at the surfaces of MgO, α-Al_2O_3, and CeO_2 containing small Rh clusters. Stoichiometric reactions are linked to a repeating loop that has produced the CPO of methane at temperatures lower than 773 K with selectivity close to 100%. These reactions occur through the formation and the thermal decomposition of hydridocarbonyl Rh clusters. Molecular aspects of stoichiometric reactions are compared with those produced under stationary conditions with flows of premixed CH_4 and O_2 at very short residence time. Comparisons show that collisions between hydridocarbonyl clusters and gaseous O_2 produce CO_2 and H_2O. IR thermography maps collected during short residence time CPO and gaseous temperature measurements are also reported. They show the existence of nonlocal thermal equilibrium between the solid and gaseous phases. © 2000 Academic Press

Key Words: **partial oxidation of methane; molecular surface chemistry; diffuse reflectance infrared spectroscopy; infrared thermography; surface temperature measurements; cluster chemistry.**

INTRODUCTION

In many regions, natural gas (NG) reserves either are flared, vented, or reinjected into oil fields or simply remain undeveloped due to uneconomic transformation and transportation costs. More than 200 basins that contain 900 underdeveloped fields have been identified. Moreover, 110×10^9 normal cubic meters (Nm^3) of NG associated with crude oil production are vented or flared worldwide every year with a detrimental effect on the environment (1).

Liquefied natural gas (LNG) and gas-to-liquid (GTL) technologies are the main routes to promote NG utilization and to avoid dispersion of NG in the atmosphere.

GTL technologies include synthesis gas production and conversion steps. Synthesis gas is a mixture whose main components are CO and H_2, and it is produced through energy-intensive processes accounting for about 60% of the overall costs of the GTL routes. The synthesis gas production technologies are (a) steam-CO_2 reforming, (b) autothermal reforming, (c) noncatalytic partial oxidation, and (d) combined reforming (2–4).

Products obtained from synthesis gas and utilized for petrochemical, chemical, and fertilizer industries are methanol, dimethyl ether, gasoline, middle distillates for diesel engines and hydrogen, ammonia, urea, formaldehyde, oxoalcohols, acetic acid, dimethyl carbonate, and others.

This work is aimed at understanding some of the physical-chemical aspects of the following reaction that could have the potential for the development of a new economic technology for the synthesis gas production:

$$CH_4 + \tfrac{1}{2}O_2 \rightarrow CO + 2H_2, \quad \Delta H^\circ = -36\,\text{kJ/mol}. \qquad [1]$$

Catalysts containing Ni (5–7) or noble metals are able to catalyze reaction [1]. Among noble metal species, Rh is unique as it avoids parasitic reactions that lead to carbon formation (8–14). Moreover, Mo_2C and WC catalysts have also been recently studied (15, 16).

Most of the work performed before 1992 considered reaction conditions with residence times (τ) between 50 and 0.1 s.

Choudary *et al.* (17–19) and Schmidt *et al.* (20–22) reported in 1992–1993 that residence times can be reduced by two orders of magnitude at values close to 10^{-3} s without decreasing conversion and selectivity values.

Schmidt and co-workers are still very active in studying the issue they reviewed in 1995 (23). They have investigated (a) the catalytic partial oxidation of various hydrocarbons (24), (b) the roles of the active metal species and of the roughness of the surfaces (25), (c) the effects of total pressure (between 1 and 6 atm) (26), and (d) the effects of reactant flow rates (27). Schmidt and Hickman have also proposed a description of the role of boundary-layer mass-transfer phenomena (28) and a microkinetic level simulation of low-pressure experiments (29).

Here we report information on molecular properties and temperature conditions of the solid–gas interphase zones produced during stoichiometric and catalytic reactions with short contact times ($\tau < 70$ ms).

The study was performed with a network of 14 experiments schematically represented in Fig. 1. The experimental

[1] To whom correspondence should be addressed. E-mail: luca.basini@snamprogetti.eni.it.

0021-9517/99 $35.00
Copyright © 2000 by Academic Press
All rights of reproduction in any form reserved.

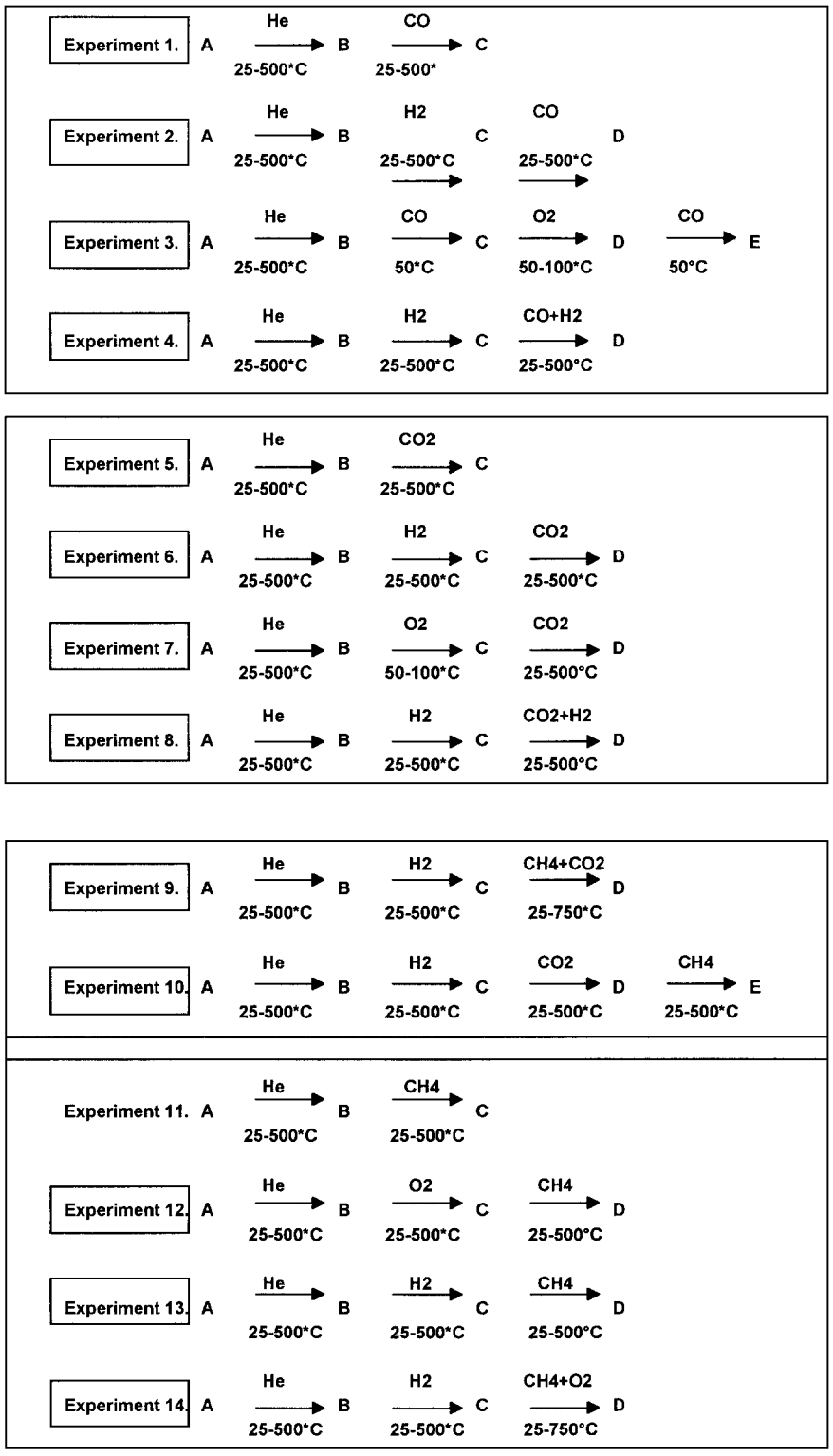

FIG. 1. Scheme of the 14 experimental sequences performed in order to investigate the Rh surface chemistry on α-Al_2O_3, MgO, and CeO_2 during CO and CO_2 methanation (experiments 1–8), CO_2 reforming and water gas shift (experiments 9 and 10), and CPO of methane (experiments 11–14.) Experiments 11–14 are dealt with here.

sequences are defined to provide information that, through a comparison and cross-linking procedure, could lead to the definition of molecular analogies between surface species produced during (i) CO and CO_2 methanation (experiments 1–8), (ii) CO_2 reformation and water–gas shift (experiments 9 and 10), and (iii) CPO of methane (experiments 11–14).

Features of experiments 1–10 were detailed in Refs. (30–33), while experiments 11–14 are described and discussed herein.

The 14 experiments were performed within a reaction chamber equipped for diffuse reflectance Fourier transform IR spectroscopy (DRIFT) and mass spectrometry; some of the experiments were repeated in a tubular reactor equipped with an IR thermograph, thermocouples, and GC analysis apparatus.

Powdered polycrystalline MgO, α-Al_2O_3, and CeO_2 containing small Rh clusters, generated through reactions with $Rh_4(CO)_{12}$ clusters, were used as solid reactants and/or catalysts.

Results showed that a cycle of solid–gas stoichiometric reactions, obtained by flowing CH_4 and O_2 in separate steps, can produce CO and H_2 at temperatures below 773 K, with selectivity close to 100%.

Moreover, it was found that short residence time CPO occurs under stationary conditions at catalyst surfaces characterized by temperatures much higher than the gas phase temperatures and higher than those expected for an adiabatic environment.

MATERIALS AND METHODS

Sample Preparation

The preparation procedure and the characterization of the cluster-containing materials were given in Refs. (30–33). The preparation method involved a solid–liquid reaction between an *n*-hexane solution of the $Rh_4(CO)_{12}$ clusters and a slurry of the powdered oxides (α-Al_2O_3 corundum and MgO periclase supplied by Aldrich (99.999 wt%), CeO_2 cerianite supplied by Johnson Matthey (99.99 wt%) in the same solvent. The oxides were Stored under N_2 to prevent interaction with moisture and CO_2. Their purity and crystalline structure were checked with optical emission arc spectroscopy and XRD analyses, and their surface areas (between 5 and 10 m^2/g) were measured with the BET method. The solids after the reaction were isolated by filtration and dried under vacuum at room temperature. DRIFT spectra of the freshly prepared powdered materials showed carbonyl absorption bands at 2008 and 2085 cm^{-1} for the Rh/MgO sample and at 2010 and 2090 cm^{-1} for the Rh/Al_2O_3. These bands were assigned to $Rh^I(CO)_2$ species formed through oxidative disaggregation of the tetrametallic clusters (34–40). $Rh^I(CO)_2$ was also detected on the Rh/CeO_2 sample (peaks at 2095 and 2010 cm^{-1}), but in this case the disaggregation of $Rh_4(CO)_{12}$ also generated a carbonyl complex with Rh in an oxidation state presumably higher than I (41, 42), which is responsible for an absorption band at 2110 cm^{-1}, and a carboxylate species with strong absorptions at 1160 and 1237 cm^{-1}.

The percentage of exposed metal atoms was between 95 and 100% and was measured by CO and H_2 selective chemisorption experiments. These were performed after the samples were pretreated in a He flow at 500°C. Dispersion was estimated assuming that each one of the exposed Rh atoms was able to coordinate one H_2 molecule or two carbonyl groups.

Freshly prepared samples were also examined by high-resolution transmission electron microscopy (HRTEM, Jeol 2000 EX, 2.5 Å resolution) that has not revealed Rh cluster formation; this sustains the assignment of IR absorption bands to $Rh^I(CO)_2$ monometallic species.

Apparatus for Spectroscopic and Spectrometric Studies

DRIFT and mass spectra in flowing gaseous environments were collected in a high-pressure high-temperature (HPHT) reaction chamber at 0.1 MPa and temperatures between 298 and 1023 K. The chamber has already been described in Refs. (30–33). Briefly, powdered samples (30 mg) were placed on a fritted tungsten disk inside a small heater at the center of the reaction chamber, whose external walls were water-cooled. Two ZnSe windows, located at the two sides of the chamber, were used for incoming and reflected radiation. A 0.5-mm chromel–alumel thermocouple inserted amid the powdered sample monitored and controlled the reaction temperature. The experimental apparatus maintained high-temperature conditions in the small reaction zone containing the catalysts and room temperature conditions in the incoming gaseous streams. The gases, after entering the reaction chamber, flowed through the hot powdered samples into an output line connected to a quadrupole mass spectrometer through a two-orifice pressure reduction sampling stage.

DRIFT spectra were recorded at a resolution of 4 cm^{-1}. Signal to noise ratios were reduced by collecting 400 scans in about 2 min.

Stoichiometric reactions were performed between 298 and 773 K in flowing atmospheres containing (a) pure He, (b) $He/H_2 = 4/1$ v/v, (c) $He/O_2 = 4/1$ v/v, (d) $He/CH_4 = 4/1$ v/v.

CPO was studied in experiment 14 using a reactant mixture with $CH_4/O_2/He = 2/1/4$ v/v.

Apparatus for Temperature Measurements with IR Thermography and Thermocouples

CPO reactions were also studied in a cylindrical tubular quartz plug flow reactor (PFR) with internal diameter 15 mm and wall thickness 1 mm. A quartz thermowell with

an internal diameter of 3 mm was placed in the center of the reactor through the catalyst bed, which was 10 mm high. Two movable chromel–alumel thermocouples were positioned inside the quartz wall at the two extreme zones of the catalytic bed. The catalyst particles (1.5 g of regular α-Al_2O_3 spheres with diameter 1 mm and containing 0.32% wt of Rh) were placed in the annular zone between the thermocouple well and the internal wall of the reactor. Reactants (H_2, N_2, O_2, CH_4) were supplied from cylinders into different lines, each equipped with mass flow meters and controllers. Product composition was monitored by gas chromatography.

An IR camera (Thermovision 900 SW/TE) was used for temperature measurement and analysis of both static and dynamic thermal patterns of the reacting catalyst. The camera has an internal compensation and self-calibration system based on two microblackbodies and four temperature sensors. It is thermoelectrically cooled and operates in the short-wave range (3–5 μm), suitable for high-temperature applications. An "HT 1" filter (cut-on 3.82 μm, cut-off 3.9 μm) increased the measurement range to 2000 K.

The system was equipped with a 20° lens (field of view $H \times V = 20^\circ \times 12.5^\circ$; spatial resolution 2.5 mrad) and a close-up lens (spatial resolution 0.32 mrad corresponding to about 250 μm). The IR camera was interfaced to a PC for the online acquisition of 12-bit digital images and data. Emissivity values were adjusted with temperature-dependent equations derived from the literature (43).

Thermodynamic Calculation and Estimates of Adiabatic Temperatures

Eqs. [2–4] were used to estimate the equilibrium temperatures (T_{WGS}, T_{SR}, T_{CR}), of the water–gas shift [5], steam reforming [6], and CO_2 reforming [7] reactions according to the procedures of Ref. (44); partial pressure values correspond to experimental product compositions:

$$T_{WGS} = \frac{-\Delta G_{WGS}}{\ln\left(P_{CO_2}P_{H_2}/P_{CO}P_{H_2O}\right)}, \quad [2]$$

$$T_{SR} = \frac{-\Delta G_{SR}}{\ln\left(P_{CO}P_{H_2}^3/P_{CH_4}P_{H_2O}\right)}, \quad [3]$$

$$T_{CR} = \frac{-\Delta G_{CR}}{\ln\left(P_{CO}^2P_{H_2}^2/P_{CH_4}P_{CO_2}\right)}, \quad [4]$$

$$CO + H_2O = CO_2 + H_2, \quad [5]$$

$$H_2O + CH_4 = CO + 3H_2, \quad [6]$$

$$CO_2 + CH_4 = 2CO + 2H_2. \quad [7]$$

Adiabatic exit temperatures for chemical systems at thermodynamic equilibrium ($T_{ad.eq.}$) were estimated using Aspen Technology software, Aspen Release 9.2.

Adiabatic exit temperatures corresponding to the experimental product compositions ($T_{ad.exp.}$) were calculated using the procedures, enthalpy, and heat capacity values given in Ref. (44).

RESULTS

DRIFT and Mass Spectrometry Measurements

Experiments 11–14 were performed using pure MgO, α-Al_2O_3, and CeO_2 and using the same oxides containing the Rh clusters. The thermal cracking of methane was the only reaction detected with pure MgO and α-Al_2O_3. Traces of CO and H_2 were detected during the interactions between CH_4 and pure CeO_2, a material known for having oxygen storage properties (45).

The reactivity observed with the samples containing Rh clusters was much more complex, and it is detailed here. Samples contained 0.1% wt of Rh, corresponding to less than 1/10 of a monolayer of $Rh_4(CO)_{12}$ clusters. Experiment 14 was repeated with samples containing higher Rh loadings.

Experiment 11: $A \xrightarrow[773\,K]{He} B \xrightarrow[773\,K]{He + CH_4} C$

DRIFT and mass spectrometry measurements were collected during the two subsequent thermal cycles between 298 and 773 K.

The monometallic Rh dicarbonyl species present at point A (see the experimental paragraph) were transformed (during the heating in He flow) into hydridocarbonyl clusters through the stoichiometric surface water–gas shift reaction [8]. The clusters were decarbonylated at temperatures higher than 474 K according to the chemical features reported in refs. (30, 32):

$$[M]\text{-O-Rh(CO)}_2 + M\text{-OH} \rightarrow [MO_xRh_yH_z(CO)_n] + CO_2, \quad M = \text{Mg, Al, Ce.} \quad [8]$$

The interactions between the decarbonylated clusters and CH_4 at $T > 573$ K produced new surface carbonyl clusters, gaseous CO, and H_2, but no CO_2 or H_2O. The volume ratios between desorbed H_2 and CO were equal to 3.8 v/v, indicating that thermal cracking (producing H_2 and surface carbon species) and partial oxidation of methane (producing CO, H_2, and surface carbonyls) occurred simultaneously.

The formation of H_2 and CO was reduced with time on stream, and the carbonyl bands also disappeared from the DRIFT spectra, due to the stoichiometric nature of the reactions.

Figures 2A and 3A show respectively the carbonyl stretching bands detected with DRIFT spectra on the

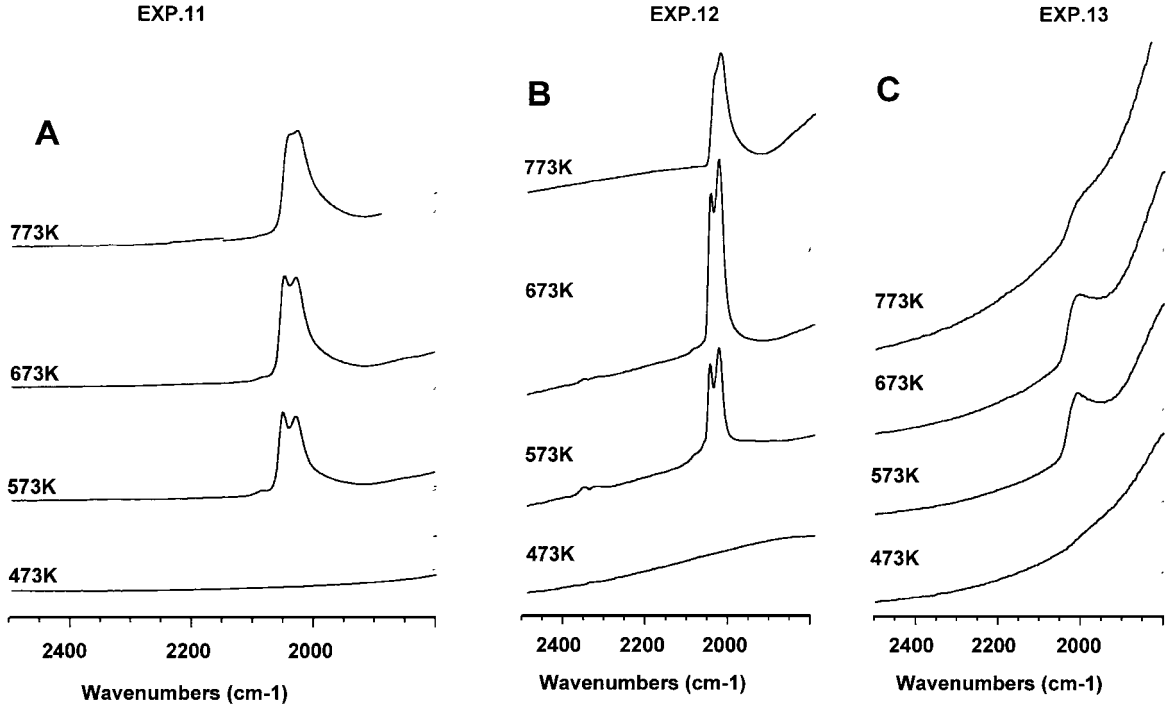

FIG. 2. Carbonyl stretching bands generated during the last steps of experiments 11, 12, and 13.

$Rh/\alpha\text{-}Al_2O_3$ sample and the temperature-dependent formation of H_2 and CO.

Experiment 12: $A \xrightarrow[773\,K]{He} B \xrightarrow[373\,K]{O_2} C \xrightarrow[773\,K]{He+CH_4} D$

This experiment investigated the reactivity between CH_4 and solid samples pretreated in He at 773 K and in O_2 flows at 373 K. Previous work showed that highly reactive surface-oxygen-containing species formed during the oxidation treatment (30–32). The existence of these species was detected through their ability to oxidize CO into CO_2 even at 298 K (see Fig. 3B showing a cycle of reactions obtained in experiment 3 (30) schematized in Fig. 1). These species also reacted with CH_4, producing CO and H_2 with a selectivity close to 100% and surface carbonyls, and enhancing the reactivity features observed during experiment 11 (see Figs. 2B and 3B). In fact, mass spectrometry detected the formation of CO and H_2 at temperatures 100 K lower than in experiment 11, and DRIFT spectrometry showed the formation of sharp and intense multiplets assigned to the selective formation of small surface carbonyl clusters.

The ratio between the volume amounts of H_2 and CO was below 2 v/v in the three examined samples, indicating that thermal cracking of methane did not occur after the oxidizing treatment.

At the end of the experiment, the cooled samples were reoxidized in O_2 flow at 373 K and again thermally treated in flowing $CH_4 + He$. The formation of carbonyl clusters and of CO and H_2 was observed again. The cycle of oxidative and reductive treatments schematized in Fig. 4A was repeated several times, showing that the reactivity features were reproducible, generating a catalytic loop that consumed CH_4 and O_2 in separate steps produce CO and H_2.

These features were common to the Rh/MgO, $Rh/\alpha\text{-}Al_2O_3$, and Rh/CeO_2 samples.

Experiment 13: $A \xrightarrow[773\,K]{He} B \xrightarrow[773\,K]{He+H_2} C \xrightarrow[773\,K]{He+CH_4} D$

This experiment investigated the interactions between CH_4 and the solids thermally pretreated at 773 K in He and H_2. The description of the reactions produced in H_2 flow is reported in Refs. (30–32). Here it is briefly mentioned that Rh–hydrido clusters formed and were detected by DRIFT spectroscopy and isotopic exchange experiments. These clusters had diameters smaller than 10 Å, as estimated by HRTEM (32).

The chemical reactions between CH_4 and the hydrido clusters are modest if compared with those observed in experiments 11 and 12. Hydrogen, the main gaseous product, was formed above 474 K together with minor amounts of CO, thus indicating the occurrence of thermal cracking of methane. Moreover, very weak and broad absorption bands were observed in the DRIFT spectra (Figs. 2C and 3C). Among the three samples examined, the Rh/CeO_2 was the one that produced the largest amount of gaseous CO and surface carbonyl clusters.

Note that the comparison between the intensity of the signals produced in the mass spectra of experiments 11, 12,

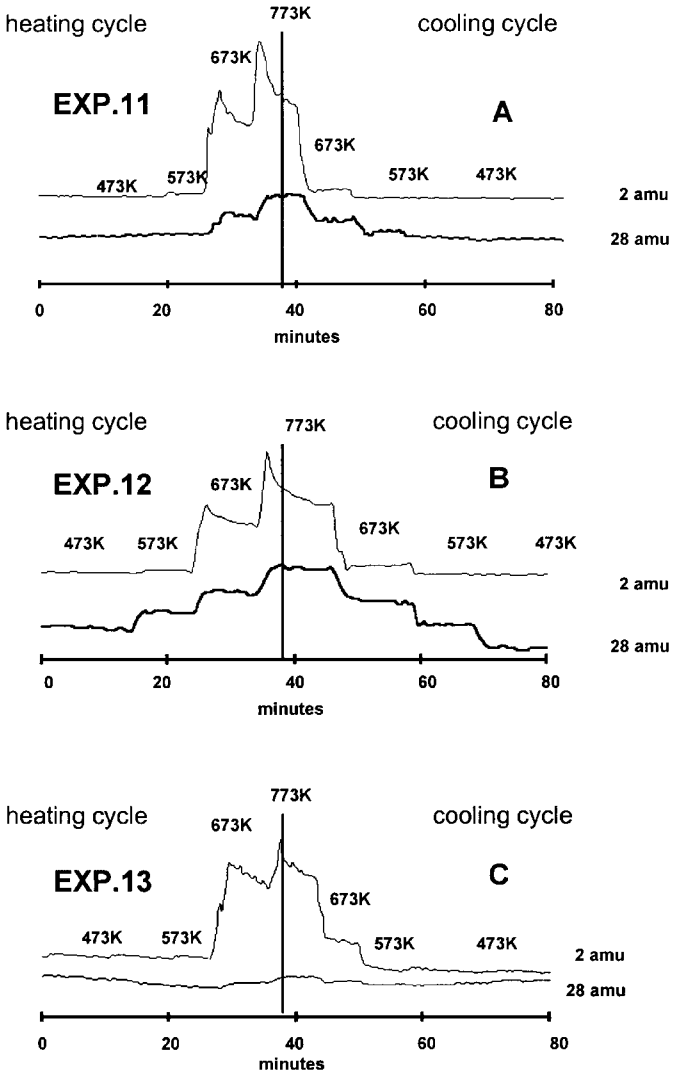

FIG. 3. Selected peak monitoring with time ($m/e = 28$ and 2) corresponding to CO and H_2 formation during the last steps of experiments 11, 12, and 13.

and 13 shows that total H_2 production was comparable in the three experiments, while CO production was highest in experiment 12 and intermediate in experiment 11, and only traces of CO were detected in experiment 13. This indicates that CO production was related to the degree of oxidation of the material surfaces.

Experiment 14: $A \xrightarrow[773\,K]{He} B \xrightarrow[573\,K]{He+H_2} C \xrightarrow[1073\,K]{He+CH_4+O_2} D$

A premixed $CH_4 + O_2 + He$ flow was admitted into the reaction chamber after two thermal treatments in He and H_2, performed as in experiment 13. Moreover, the last step of this experiment was performed at two contact times corresponding to 7.2 and 72 ms and with samples having Rh loadings of 0.1 and 0.8 wt%.

Mass spectroscopy analysis showed that methane conversion and intensity of the signal of CO and H_2 increased

TABLE 1*

T (K)	Rh/Al_2O_3	Rh/MgO	Rh/CeO_2
473	—	2345 w	2340 w
573	2349 w	2349 w	2349 w
673	2349 mw, 2014 mw	2349 w	2349 m, 2015 mw
773	2349 m, 2023 s	2349 mw	2349 s, 2018 m
873	2349 m, 2145 w, 2017 s	2349 m	2349 s, 2145 w, 2016 mw
973	2349 m, 2145 w, 2004 m	2349 s, 2147 w	2349 s, 2145 w, 2000 w
1023	2349 m, 2145 w, 1990 mw	2349 s, 2147 w	2349 s, 2145 w, 1990 w
973	2349 m, 2145 w, 1990 mw	2349 s, 2147 w	2349 s, 2145 w. 2000 w
873	2349 m, 2145 w, 2008 mw	2349 s	2349 s, 2145 w, 2005 w
773	2349 m, 2017 mw	2349 s	2349 s, 2000 w
673	2349 mw, 2017 mw	2349 w	2349 s, 2010 mw
573	2349 w	2349 w	2349 w
473	—	2345 w	2342 w

* $\tau = 72$ ms.

monotonically with temperature between 298 and 1073 K at $\tau = 72$ ms. The intensity of the signals of CO_2 and H_2O reached a maximum value at 673 K (Fig. 5A). Surface carbonyl clusters formed at temperatures between 673 and 1073 K. IR bands appeared stronger and sharper during the heating cycles (Fig. 5B). These general features were common to all of the three samples examined, However, some differences occurred in the intensity and positioning of the CO stretching bands of the surface carbonyl complexes. These differences are reported in Table 1.

Figures 5A,B and 6A,B show the product composition and the carbonyl bands, detected with the Rh/α-Al_2O_3 sample containing 0.1 wt% Rh.

The figures show that reduction of τ from 72 to 7.2 ms caused an increase in the CO_2 and H_2O produced and the occurrence of temporal oscillations in chemical reactivity (Fig. 6A). Surface carbonyl formation was also reduced. However, the reactivity features were not modified by

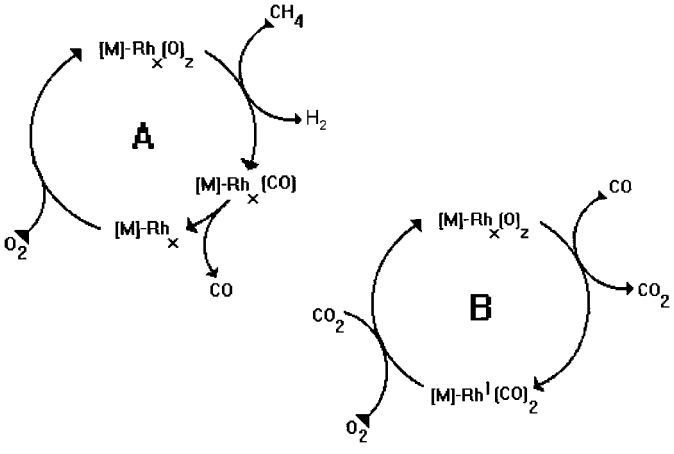

FIG. 4. Scheme of the identified molecular features produced (A) during a cyclic sequence of surface stoichiometric reactions realized in experiment 12 and (B) in experiment 3 as described in Ref. (30).

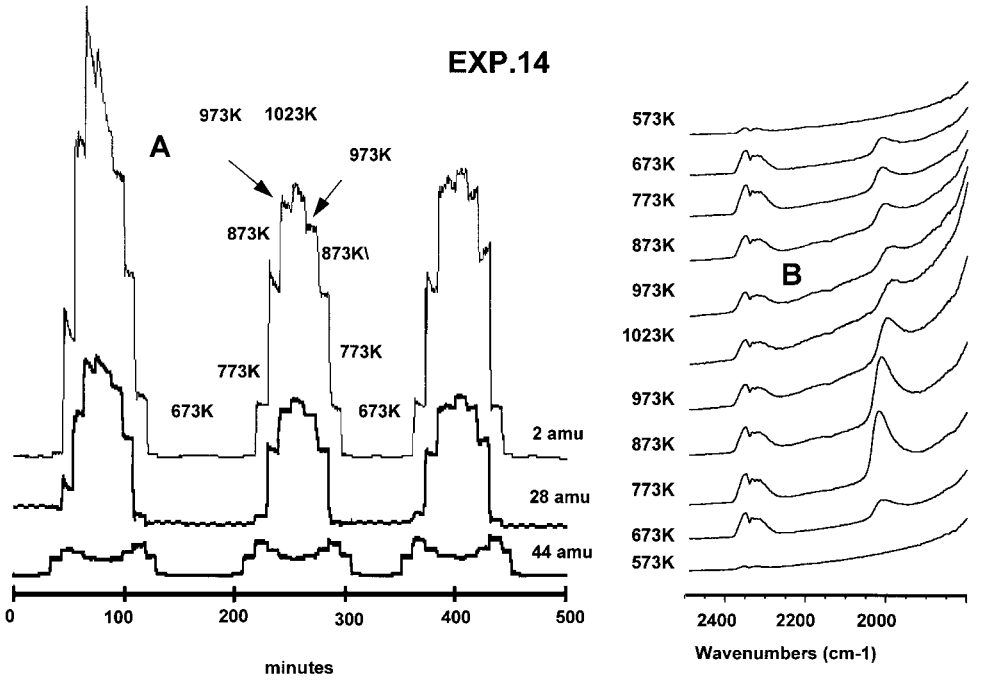

FIG. 5. Mass and DRIFT spectra collected during the last step of experiment 14 performed at a residence time of 72 ms with the Rh/α-Al_2O_3 sample (0.1% wt of Rh). (A) Selected peak monitoring with time ($m/e = 2, 28, 44$) corresponding to H_2, CO, and CO_2 formed during three consecutive thermal cycles between 298 and 1023 K in flowing CH_4 and O_2 streams; (B) DRIFT spectra collected during the second thermal cycle.

reducing the residence time from 72 to 7.2 ms when catalysts containing 0.8 wt% Rh were used.

Experiment 14 was repeated in a quartz plug flow reactor (PFR) that contained 1.5 g of α-Al_2O_3 spherical pellets ($\phi = 1$ mm) with an overall Rh loading of 0.32 wt%. The catalyst was prepared by reacting the α-Al_2O_3 spherical pellets with an *n*-hexane solution of $Rh_4(CO)_{12}$ by the same procedure used for the powdered materials. DRIFT spectra

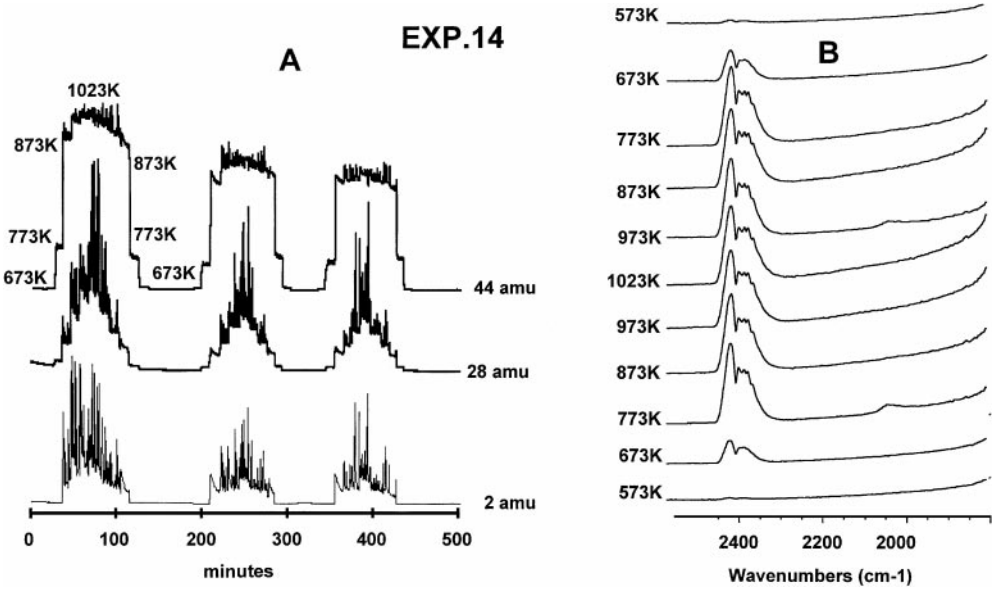

FIG. 6. Mass and DRIFT spectra collected during the last step of experiment 14 performed at a residence time of 7.2 ms with an Rh/α–Al_2O_3 sample (0.1% wt of Rh). (A) Selected peak monitoring with time ($m/e = 2, 28, 44$) corresponding to H_2, CO, and CO_2 formed during three consecutive thermal cycles between 298 and 1023 K in flowing CH_4 and O_2 streams; (B) DRIFT spectra collected during the second thermal cycle.

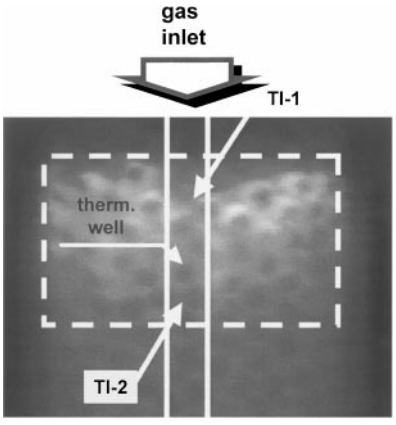

FIG. 7. IR thermography image of the catalytic bed collected under reaction conditions. The image also shows the positions of the thermocouples (Tl1 and Tl2).

TABLE 2

Contact time (ms)	7.2
O_2/CH_4 (v/v)	0.5
$T_{\text{in gas}}$ (K)	298
$T_{\text{in surf.}}$ (K)	1380
$T_{\text{out gas}}$ (K)	930
$T_{\text{out surf.}}$ (K)	1313
% conv. CH_4	86.1
% conv. O_2	100
$T_{\text{F CH}_4}$ (s^{-1})	188
$T_{\text{F O}_2}$ (s^{-1})	94
% sel. CO	95.7
% sel. H_2	93.8
H_2/CO (v/v)	1.96
$T_{\text{eq. WGS}}$ (K)	1226
$T_{\text{eq. steam ref.}}$ (K)	1026
$T_{\text{eq. CO}_2\text{ ref.}}$ (K)	1023
$T_{\text{ad.eq.}}$	1035
$T_{\text{ad.exp.}}$	1034

of the freshly prepared samples showed the same absorption bands observed on the powdered samples and assigned to $Rh^1(CO)_2$ surface species (see also Materials and Methods). Note that the species were grafted onto a 200-μm thick external cortex of the pellets and there the concentration of Rh corresponded to 0.52 wt%.

Reaction ignition was achieved by impinging a hot air beam on the external walls of the reactor confined with the catalytic bed. After ignition, the hot air beam was switched off and reactions remained self-sustained using a feedstock with $CH_4/O_2/N_2 = 8/4/1$ v/v maintained at 298 K.

Figures 7 and 8 show respectively an IR thermograph image of the reacting environment (also indicating the positioning of the thermocouples) and a plot of the axial temperature profiles of the solid and gaseous phases. Note that surface temperatures increase steeply at the beginning of the bed and then remain nearly constant above 1350 K, while gas temperatures increase gradually (between 850 and 980 K) but remain much lower than surface temperatures. IR thermography also shows small radial temperature gradients.

Table 2 includes (a) conversion, selectivity, and turnover frequency (TF) data, (b) measured surface and gas temperatures ($T_{\text{surf.}}$ and T_{gas}), (c) calculated equilibrium temperatures (T_{WGS}, T_{SR}, T_{CR}), and (d) calculated adiabatic temperatures ($T_{\text{ad. exp.}}$, $T_{\text{ad. eq.}}$) corresponding to the experimental and equilibrium product mixtures (see Materials and Methods).

TF values of Table 2 were estimated by determining the percentage of exposed Rh atoms on a sample discharged

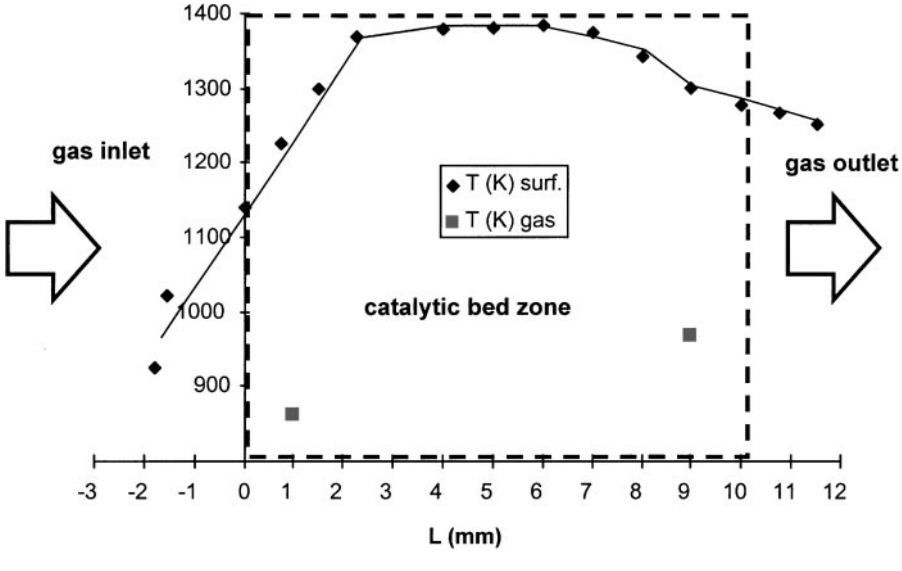

FIG. 8. Surface and gas phase temperature profiles measured respectively with IR thermography with thermocouples.

after 100 h of reaction. This percentage, measured through H_2 chemisorption, was equal to 65% (note that dispersion measured on the freshly prepared material corresponded to 95%; see also Materials and Methods). Higher dispersion (78%) was estimated through CO chemisorption. However, DRIFT spectra of the spent materials exposed to CO showed bands that formed and changed with time. This indicates that during CO chemisorption, restructuring and a partial disaggregation of the metal aggregates should have occurred.

HRTEM analysis did not reveal the presence of Rh clusters on the fresh samples, but the same analysis performed on the spent catalyst revealed the presence of a large number of Rh clusters whose diameters were between 10 and 60 Å.

The equilibrium temperature of the water gas shift (T_{WGS}) reaction [4] was higher than the steam reforming (T_{SR}) and the CO_2 reforming (T_{CR}) equilibrium temperatures; this indicates that the short residence time CPO process occurred under kinetically controlled conditions.

Interestingly, comparisons between calculated and experimental values show that surface temperatures ($T_{surf.}$) were higher than adiabatic temperatures, which, in turn, were higher than gas temperatures (T_{gas}).

Moreover, it was found that the equilibrium temperatures T_{WGS}, T_{SR}, and T_{CO_2} were higher than T_{gas} but lower than T_{surf}.

T_{SR} and T_{CO_2} were also very close to the adiabatic temperatures, while T_{WGS} was higher.

In conclusion, the experimental and calculated temperature values are ordered as follows:

$$T_{surf.} > T_{WGS} > T_{SR}, T_{CR} \cong T_{ad.exp.}, T_{ad.eq.} > T_{gas}.$$

DISCUSSION

Experiments 11 and 12 showed that stoichiometric reactions between gaseous CH_4 molecules and surface sites containing Rh and O species produced H_2 and CO through the decomposition of Rh hydridocarbonyl clusters.

These reactions occurred at moderate temperatures (lowest value 573 K in experiment 12), with selectivity toward CO and H_2 close to 100%, and were favored by a pre-oxidizing treatment of the surfaces but were depressed by a pretreatment in H_2 flow.

Moreover, the repetition of a sequence of stoichiometric reactions generated a catalytic loop that consumed CH_4 and O_2 in separate steps and produced CO and H_2 (see Fig. 4A and Ref. (46)).

The direct formation of CO and H_2 was also observed in molecular dynamics studies performed under nearly collision-free conditions. These studies were aimed at generating primary product molecules (at an equivalent pressure of ≅0.1 Pa) desorbing from the surfaces without colliding with incoming reactants, thus carrying with themselves any excess energy content resulting from the occurrence of uncompleted energy accommodation processes.

Kunimori *et al.* (48–50) studied the oxidation of C2–C4 hydrocarbons with this experimental approach. They found that CO and H_2 formed as primary products with extremely high selectivity at surface temperatures higher than 1000 K, for which thermally activated desorption of primary reaction products was further favored over total oxidations (18, 26) not thermally activated. We obtained analogous results by studying the partial oxidation of CH_4 (51) even at extremely high O_2/CH_4 molar ratios ($O_2/CH_4 = 0.5$–5 v/v).

In this experimental work total oxidation phenomena occurred only when CH_4 and O_2 flowed simultaneously through the reaction environment (experiment 14). Moreover, an increase of the selectivity toward total oxidation products was followed by an intensity decrease of the IR absorption bands of the surface carbonyl species and vice versa.

These findings indicate that CO_2 and H_2O were produced by collisions between surface precursors of primary partial oxidation products, namely, hydridocarbonyl species and gaseous oxygen molecules (52).

Results of experiment 14 in the DRIFT chamber also showed that residence time, Rh loading, and surface temperature effects are strongly related and can be investigated to determine the prevalence of total or partial oxidation phenomena.

A 10-fold reduction of residence time from 72 to 7.2 ms caused a reduction of the selectivity toward synthesis gas, apparently under the same T and P conditions. However, the selectivity change occurred when catalysts containing 0.1% wt of Rh were used but not when catalysts containing 0.8% wt of Rh were used.

This finding is explained by considering the occurrence of variations of the balance between the rates of heat production and heat dispersion. In more detail, it is observed that the larger the number of reacting Rh-containing sites, the larger should the achievable value of the rate of heat production per unit surface be. We believe that at 7.2 ms and 0.8% wt of Rh loading the rate of heat production could have balanced the surface cooling produced by convection (note that the reactant mixture contained large amounts of He as diluent gas; see also Materials and Methods). We hypothesize that this compensation effect could not be obtained at 7.2 ms with Rh loading corresponding to 0.1% wt.

In synthesis, higher surface temperatures should have been reached with higher Rh loadings, and the temperature-dependent competition between thermally activated desorption of CO and H_2 and not thermally activated total oxidation processes should explain the reactivity differences.

Surface temperature variations could not be detected with thermocouple measurements in the reaction chamber equipped for DRIFT and mass spectrometry. However, the IR thermography experiments showed that surface and gas

temperatures can differ by more than 300 K (see Table 2 and Figure 8).

Other authors have made experimental observations with optical pyrometers and discussed the occurrence of hot spot phenomena that generate reaction environments with high local temperatures that are difficult to detect with thermocouple measurements (53–56). The same authors also have discussed the relevance of these effects in determining nonequilibrium reactivity features.

Surface temperature values higher than the adiabatic ones indicate that the reacting interphase zones have been characterized by excess enthalpy content.

The generation of environments with an excess enthalpy content is often related to conditions where mass transfer proceeds more rapidly than heat transfer does. However, in our experiments, Lewis number values (which represent ratios between heat transfer and mass transfer) have been above 1. This excludes heat-transfer limitation as a cause of temperature increase. Instead, the excess enthalpy content of the interphase zones may result from internal recirculation or recuperation of heat from the product molecules towards the reactants.

Weinberg *et al.* introduced this concept in the late 1960s (57–61) while studying the properties of high-efficiency combustors. The schemes of Fig. 9A proposed by these authors show how heat recirculation can be obtained by convection with an external heat exchanger. Figure 9B shows a qualitative enthalpy vs distance diagram, corresponding to the conditions schematized in Fig. 9A. The enthalpy vs distance diagram also holds for conditions where internal energy recirculation is occurring, through radiation and conduction, within a catalytic bed.

Obviously, in the absence of heat recirculation the final adiabatic temperature in a homogeneous phase partial oxidation process would be given for a given mass of mixture by

$$Q_{\mathrm{CPO}} = \int_{T_\mathrm{i}}^{T_\mathrm{f}} C_\mathrm{p}\, dT, \qquad [9]$$

$$T_\mathrm{f} = \frac{Q_{\mathrm{CPO}}}{C_\mathrm{P}} + T_\mathrm{i}, \qquad [10]$$

where Q_{CPO} is the heat released by the partial oxidation reactions, C_p is the heat capacity of the products at constant pressure, and T_i and T_f are the initial and final temperature values, respectively.

When a heat recuperation mechanism is established and some enthalpy is transferred from the product gases into the reactants, the reaction temperature T_R would be higher than the final temperature T_f according to the following equations, where Q_R represents the heat recuperation term:

$$Q_{\mathrm{CPO}} + Q_\mathrm{R} = \int_{I_\mathrm{i}}^{T_\mathrm{f}} C_\mathrm{p}\, dt + \int_{T_\mathrm{f}}^{T_\mathrm{R}} C_\mathrm{p}\, dt, \qquad [11]$$

$$T_\mathrm{R} = \frac{Q_{\mathrm{CPO}} + Q_\mathrm{R}}{C_\mathrm{P}} + T_\mathrm{i}. \qquad [12]$$

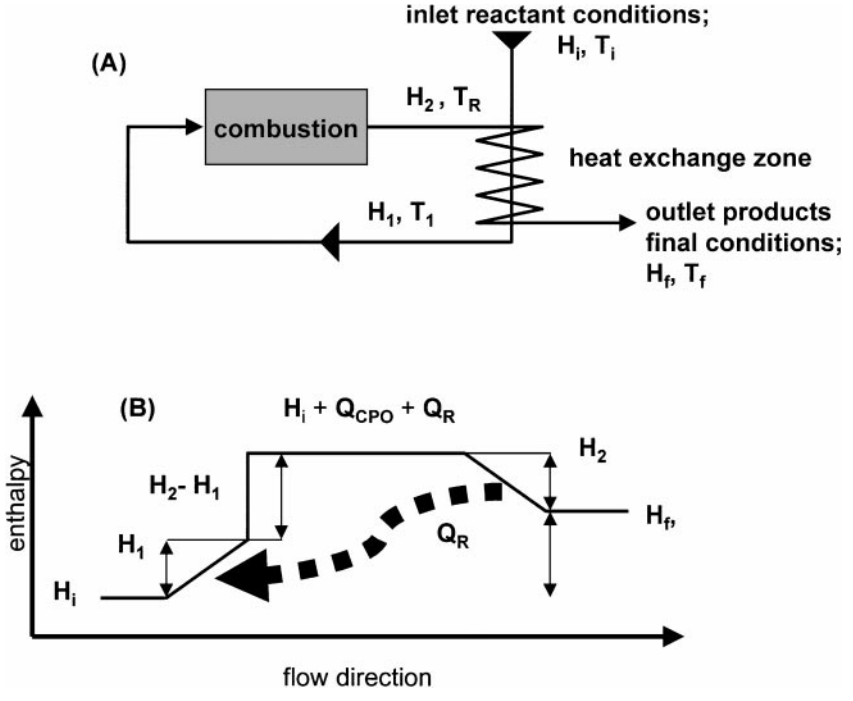

FIG. 9. (A) Scheme of a one-phase combustor with external heat recuperation from the products and preheating of the feedstock. (B) Enthalpy vs distance diagram for the same combustor; the diagram holds also in the case of internal heat recuperation phenomena occurring through a ceramic bed (62).

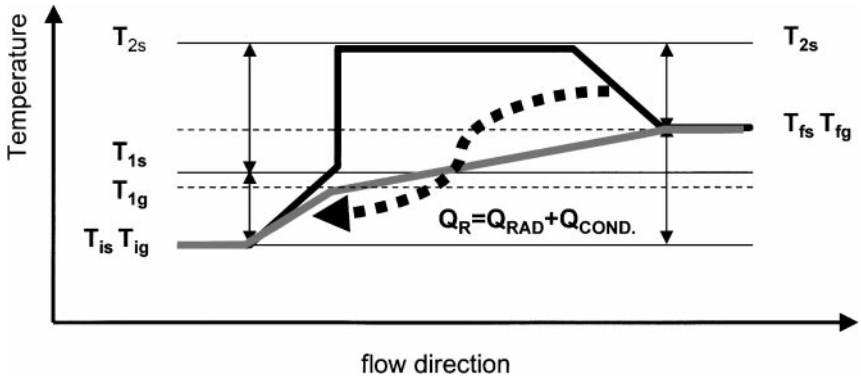

FIG. 10. Qualitative scheme of the temperature vs distance diagrams for the solid and gaseous phases (solid phase, solid line; gas phase, dotted line) produced during CPO under stationary flow conditions in an adiabatic reactor. T_{iG} and T_{iS} are inlet temperatures of the gas and solid; T_{1G}, T_{1S}, ignition temperatures affected by the heat recuperation term (Q_R); T_{2G}, T_{2S}, reaction temperatures; T_{fG}, T_{fS} final exit temperatures.

These simple concepts have found technological applications in flameless total combustion processes, used for VOC abatement or for thermal treatment of plastic materials and in furnaces for stainless steel production. Reference (62) is a comprehensive review of activities in this field.

In the case of the heterogeneous short residence time CPO the large difference between gas and surface temperatures (see Fig. 8) and the very large temperature gradients in the interlayer zones allows us to assume that reactions remain confined at the solid surfaces while the gas phase is chemically cool. Moreover, it is observed that even homogeneous phase reactions should remain confined in a thin boundary zone where collisions with the surfaces have a quenching effect on the propagation of radical reactions in the gaseous phase.

Experiments have also shown that surface temperatures rise steeply to the highest values in the very initial portion of the catalytic bed and remain nearly constant, while gas temperatures gradually increase from the inlet to the exit zones.

We explain the steep temperature increase at the beginning of the catalytic bed and the flatness of the axial and radial temperature profiles of the solid, but not of the gas, by assuming that thermal energy is transferred from hotter to cooler surface zones.

Radiative heat transfer, occurring through the confining catalyst particles, with a minor contribution of heat conduction, can be considered responsible for this phenomenon.

Radiative heat transfer affects mainly surface temperature properties since the solid surfaces emit, absorb, and scatter the radiative heat much better than the gaseous phase. The gas is gradually heated along the bed due to desorption of hot reaction products and due to collisions with the hot surfaces.

The temperature difference between solid and gas clearly indicates the existence of a nonlocal thermal equilibrium. Combustion science models of flame stabilization and multimode heat transfer in inert prorous media (63) describes such conditions with separate energy equations for the solid and gas phases.

Figure 10 includes a qualitative picture of the temperature variations that would occur according to the above-reported assumptions; the scheme is a modification of Fig. 9B.

In more detail, Fig. 10 shows that in an adiabatic environment, the temperature of the solid phase rises with respect to the inlet value (T_{iS}) due to recuperation, through conduction and radiative means, of a portion (Q_R) of the chemical heat (Q_{CPO}) produced by the reaction, while the temperature of incoming gaseous reactants (T_{iG},) rises due to collisions with the hot surfaces. Reaction ignition then occurs at T_{1S}, and a temperature (T_{2S}) that exceeds the final adiabatic temperatures (T_{fS}, T_{fG}) is reached.

CONCLUSIONS

Experiments performed in a reaction chamber equipped with IR and mass spectrometry have shown that CO and H_2 are produced as primary reaction products with selectivity close to 100% by alternating reactions with flowing streams of CH_4 and O_2. When CH_4 and O_2 were admitted simultaneously into the reaction environment, CO_2 and H_2O were also formed through reactions involving Rh hydridocarbonyl species and gaseous O_2 molecules. CO_2 and H_2O formation was reduced at high surface temperatures, suggesting that at high temperatures thermally activated desorption of primary reaction products (CO, H_2) prevailed over total oxidation.

IR themography and thermocouple measurements showed large temperature gradients between surfaces and gaseous phases. Comparisons between experimental temperatures and calculated adiabatic temperatures showed that short residence time CPO occurred in an excess enthalpy interphase environment. This environment is probably responsible for the high reaction rates.

A description of the mechanisms that cause such phenomena has been proposed. This description has analogies with that proposed for flameless total oxidation processes and considers heat recirculation phenomena determining the transfer of energy through the catalyst bed from the products toward the incoming reactants.

ACKNOWLEDGMENTS

We thank L. D. Schmidt, J. Rostrup-Nielsen, K. Aasberg-Petersen, and J. H. Bak-Hansen for time spent in fruitful discussions and G. L. Haller of Yale University for introducing us to the complex word of molecular dynamics. In conclusion, we thank P. Visioli and G. Lupi for their technical assistance in performing the IR thermography experiments.

REFERENCES

1. Agbim, A., *in* "Proceedings of the Conference 'Monetizing Stranded NG Reserves 98,' San Francisco, December 14–16, 1998," *available at* http://www.remotegasstrategies.com.
2. Rostrup-Nielsen, J. R., *in* "Catalysis Science and Technology" (J. R. Anderson and M. Boudart, Eds.), Vol. 5, pp 1–118. Springer-Verlag, Berlin, 1984.
3. Christensen, T. S., and Primdahl, I. I., *Hydrocarbon Proc., Int. Ed.* **73**, 39 (1994).
4. Rostrup-Nielsen, J. R., *Catal. Today* **18**, 305 (1993).
5. Prettre, M., Eichner, C., and Perrin, M., *Trans. Faraday Soc.* **43**, 355 (1946).
6. Dissanayake, D., Rosinek, M. P., Kharas, K. C. C., and Lunsford, J. H., *J. Catal.* **132**, 117 (1991).
7. Gavalas, G. R., Phichitcul, C., and Voecks, G. E., *J. Catal.* **88**, 54 (1984).
8. Hockmuth, J. K., *Appl. Catal. B: Environ.* **1**, 89 (1992).
9. Walter, K., Buyevskaya, O. V., Wolf, D., and Baerns, M., *Catal. Lett.* **29**, 261 (1994).
10. Ashcroft, A. T., Cheetham, A. K., Foord, J. S., Green, M. L. H., Grey, C. P., Murrel, A. J., and Vernon, P. D. F., *Nature* **352**, 225 (1991).
11. Tsang, S. C., Claridge, J. B., and Green, M. L. H., *Catal. Today* **23**, 3 (1995).
12. Vernon, P. D. F., Green, M. L. H., Cheetham, A. K., and Ashcroft, A. T., *Catal. Today* **13**, 417 (1992).
13. Pirier, M. G., Jean, G., and Poirier, M. P., *Stud. Surf. Sci. Catal.* **73**, 359 (1992).
14. Wang, D., Dewaele, O., De Groote, A. M., and Froomant, G. F., *J. Catal.* **159**, 418 (1996).
15. York, A. P. E., Claridge, J. B., Marquez-Alvarez, C., Brungs, A. J., and Green, M. L., *Prepr. Am. Pop. Chem. Soc. Div. Fuel Chem.* **42**(2), 606 (1997).
16. York, A. P. E., Claridge, J. B., Marquez-Alvarez, C., Brungs, A. J., and Green, M. L., *Chem. Commun.* 39 (1997).
17. Choudary, V. R., Mamman, A. S., and Sansare, S. D., *Angew. Chem., Int. Ed. Engl.* **31**, 1189 (1992).
18. Choudary, V. R., Rajput, A. M., and Rane, V. H., *J. Phys. Chem.* **96**, 8686 (1992).
19. Choudary, V. R., Rajput, A. M., and Prabhakar, B., *J. Catal.* **139**, 326 (1993).
20. Hickman, H., and Schmidt, L. D., *J. Catal.* **138**, 267 (1992).
21. Huff, H., and Schmidt, L. D., *J. Phys. Chem.* **97**, 11815 (1993).
22. Hickman, D. A., and Schmidt, L. D., *Science* **259**, 343 (1993).
23. Bharadwaj, S. S., and Schmidt, L. D., *Fuel Process. Technol.* **42**, 109 (1995).
24. Veser, G., and Schmidt, L. D., *AIChE J.* **42**, 177 (1996).
25. Bharadwaj, S. S., and Schmidt, L. D., *J. Catal.* **155**, 403 (1995).
26. Dietz, A. G., and Schmidt, L. D., *Catal. Lett.* **33**, 15 (1995).
27. Witt, P. M., and Scmidt, L. D., *J. Catal.* **163**, 465 (1996).
28. Hickman, D. A., and Schmidt, L. D., *J. Catal.* **136**, 300 (1992).
29. Hickman, D. A., and Schmidt, L. D., *AIChE J.* **39**(7), 1164 (1993).
30. Basini, L., Marchionna, M., and Aragno, A., *J. Phys. Chem.* **23**, 9431 (1992).
31. Basini, L., and Aragno, A., *J. Chem. Soc., Faraday Trans.* **90**(5), 787 (1994).
32. Basini, L., and Sanfilippo, D., *J. Catal.* **157**, 162 (1995).
33. Basini, L., Aragno, A., and Vlaic, G., *Catal. Lett.* **39**, 49 (1996).
34. Yates, J. T., Jr., Duncan, T. M., Worley, S. D., and Waugan, R. W., J, *J. Chem. Phys.* **70**, 1219 (1979).
35. Smidt, A. K., Hugues, F., Theolier, A., Basset, J.-M., Ugo, R., Zanderighi, G.-M., Bilhou, J. L., Bilhou-Bougnol, V., and Graidon, W. F., *Inorg. Chem.* **18**, 3104 (1979).
36. Rice, C. A., Worley, S. D., Curtis, C. W., Guin, J. A., and Tarrer, A. R., *J. Chem. Phys.* **74**, 6487 (1981).
37. Yang, A. C., and Garland, C. W., *J. Phys. Chem.* **61**, 1504 (1957).
38. Basu, T., Panayotov, D., and Yates, J. T., Jr., *J. Am. Chem. Soc.* **110**, 2074 (1988).
39. van't Blik, H. F., van Zon, J. B. A., Huizinga, T., Konisberger, D. C., and Prins, R., *J. Phys. Chem.* **89**, 4783 (1985).
40. Wang, H. P., and Yates, J. T., Jr., *J. Catal.* **89**, 79 (1984).
41. Wey, J. P., Neely, W. C., and Worley, S. D., *J. Catal.* **134**, 378 (1992).
42. Kiss, J. T., and Gonzales, R. D., *J. Phys. Chem.* **88**, 898 (1984).
43. "The Oxide Handbook" (G. V. Samsonov, Ed.). IFI/Plenum, New York, 1982.
44. Kjaer, J., *in* "Computer Methods in Gas Phase Thermodynamics." Haldor Topsøe, Vedbaek, 1972.
45. Trovarelli, A., *Catal. Rev. Sci. Eng.* **38**, 439 (1996).
46. This reactivity has some links with that already investigated within this research program and described by other authors (47) and by us (35, 37), a reactivity that concerns the cyclic formation and oxidation of surface Rh carbonyls to reduce CO_2 (see Fig. 4B).
47. Mc Millan, J. W., Fischer, H. E., and Schwartz, J., *J. Am. Chem. Soc.* **113**, 4014 (1991).
48. Watanabe, K., Uetsuka, H., Ohnuma, H., and Kunimori, K., *Stud. Surf. Sci. Catal.* **101**, 891 (1996).
49. Uetsuka, H., Watanabe, K., Iwade, T., and Kunimori, K., *J. Chem. Soc., Faraday Trans.* **91**, 1801 (1995).
50. Kunimori, K., Uetsuka, H., Iwade, T., Watanabe, T., and Ito, S., *Surf. Sci.* **283**, 58 (1993).
51. Experiments performed with G. L. Haller and C. Wey at the Department of Physical Chemistry, Yale University.
52. Note that the reaction chamber equipped with DRIFT and mass spectrometry (see also the experimental paragraph) and the dilution of the reactant gases with He did not allow the oxidation reactions to propagale in the gaseous phase, and both total and partial oxidation products were produced by heterogeneous reactions.
53. Dissanake, D., Rosinek, M. P., and Lunsford, J. H., *J. Phys. Chem.* **97**, 3644 (1993).
54. Chang, Y. F., and Heinemann, H., *Catal. Lett.* **21**, 215 (1993).
55. Matsumura, Y., and Moffat, J. B., *Catal. Lett.* **24**, 59 (1994).
56. Basile, F., Basini, L., D'Amore, M., Fornasari, G., Guarinoni, A., Matteuzzi, D., Del Piero, G., Trifirò, F., and Vaccari, A., *J. Catal.* **173**, 247 (1998).
57. Hoffamnn, J. G., Echigo, R., Yoshida, H., and Tada, S., *Combust. Flame* **111**, 32 (1997).
58. Weinberg, F. J., "Advanced Combustion Methods," p. 183. Academic Press, San Diego, 1988.
59. Loyd, S. A., and Weinberg, F. J., *Nature* **251**, 48 (1974).
60. Fox, J. S., *Comb. Sci. and Techn.* **12**, 147 (1976).
61. Weinberger, F. J., *Nature* **233**, 239 (1971).
62. Howell, J. R., Hall, M. J., and Ellzey, J. L., *Prog Energy Combust. Sci.* **22**, 121 (1996).
63. Sathe, S. B., Peck, R. E., and Tong, T. W., *Combust. Sci. Technol.* **70**, 93 (1990).